Acta Astronautica 140 (2017) 225–234

Contents lists available at ScienceDirect

Acta Astronautica

journal homepage: www.elsevier.com/locate/actaastro

Soft landing on an irregular shape asteroid using Multiple-Horizon Multiple-Model Predictive Control

MohammadAmin AlandiHallaj, Nima Assadian *

Department of Aerospace Engineering, Sharif University of Technology, Tehran, Iran

ARTICLE INFO

Keywords:
Asteroid Landing
Model Predictive Control
Predictive Path Planning
Multiple-Horizon Multiple-Model Predictive Control

ABSTRACT

This study has introduced a predictive framework including a heuristic guidance law named Predictive Path Planning and Multiple-Horizon Multiple-Model Predictive Control as the control scheme for soft landing on an irregular-shaped asteroid. The dynamical model of spacecraft trajectory around an asteroid is introduced. The reference-landing trajectory is generated using Predictive Path Planning. Not only does the presented guidance law satisfy the collision avoidance constraint, but also guarantees the landing accuracy and vertical landing condition. Multiple-Horizon Multiple-Model Predictive Control is employed to make the spacecraft track the designed reference trajectory. The proposed control approach, which is a Model Predictive Control scheme, utilizes several prediction models instead of one. In this manner, it heritages the advantages of optimality and tackling external disturbances and model uncertainties from classical Model Predictive Control and at the same time has the advantage of lower computational burden than Model Predictive Control. Finally, numerical simulations are carried out to demonstrate the feasibility and effectiveness of the proposed control approach in achieving the desired conditions in presence of uncertainties and disturbances.

1. Introduction

Exploration of small solar system bodies such as asteroids has been recently attracting scientific community's attentions. The main reason making the issue of landing on these irregular bodies interesting is the possibility of achieving valuable information of the process of formation and evolution of the solar system [1]. Moreover, since some asteroids may contain resources including water, breathable air or useful materials to use as fuel and materials for space construction, landing on asteroids and comets might be a noteworthy and essential solution of the future long space missions [2]. NEAR (Near Earth Asteroid Rendezvous) Shoemaker succeeded in touching down on Eros asteroid on 12 February 2001, which was the first soft landing on an asteroid [3]. The main objective of Hayabusa that landed on 25143 Itokawa in 2005 was to return material samples to the Earth [4]. Moreover, it studied the asteroid's shape, density, composition and spin rate. The Rosetta Lander, Philae, was the first probe which landed on a comet; 67P. It landed on 12 November 2014 to initiate its scheduled science mission, which included the determination of the chemical components and investigation of the comet activities [5].

Generally, asteroids have irregular shapes with unknown gravitational field, are small in comparison with the main planets of the solar system, and have rotational motion. The shape- and gravitational-related uncertain characteristics along with highly disturbed environment make the landing problem complicated and challenging. The most important uncertainty, which might have adverse effects on the control system, is the rapidly variable gravity field of the asteroid (with respect to the main planets of the solar system) in terms of intensity and direction in an inertial reference frame. Therefore, a nonlinear control framework with robust characteristics should be considered to deal with uncertainties and disturbances and guarantee the landing on the asteroid safely and successfully.

The mentioned challenges have made the landing problem on asteroids receive significant attention over the past years. Lafontaine investigated the autonomous guidance, navigation, and control algorithm of landing on an asteroid [6]. Kluever designed the comet rendezvous mission using solar electric propulsion spacecraft [7]. A variable structure control method as the guidance control law was employed by Liaw et al. for 2D (two-dimensional) rendezvous missions [8]. Similarly, three-dimensional rendezvous missions were studied in Ref. [9]. A proportional guidance law using terminal conditions was introduced by Cui et al. [10]. Two autonomous optical navigation schemes based on NLS (Nonlinear Least Squares) and EKF (Extended Kalman Filter) for pinpoint landing of spacecraft on asteroids were considered in Ref. [11]. Li et al.

* Corresponding author.
E-mail addresses: amin_hallaj@ae.sharif.ir (M. AlandiHallaj), assadian@sharif.edu (N. Assadian).

http://dx.doi.org/10.1016/j.actaastro.2017.08.019
Received 13 June 2017; Received in revised form 15 August 2017; Accepted 18 August 2017
Available online 24 August 2017

Abbreviations

EKF	Extended Kalman Filter
LASSO	Least Absolute Shrinkage and Selection Operator
MHMM-PC	Multiple-Horizon Multiple-Model Predictive Control
MPC	Model Predictive Control
NEAR	Near Earth Asteroid Rendezvous
NLS	Nonlinear Least Squares
N-MPC	Nonlinear Model Predictive Control
OBMPC	One-Bit Processing Based Model Predictive Control
PD	Proportional–Derivative
PDF	Probability Distribution Function
PPP	Predictive Path Planning
PWPF	Pulse-Width Pulse-Frequency
SQP	Sequential Quadratic Programming
2D	Two-Dimensional

examined PWPF (Pulse-Width Pulse-Frequency) guidance control based on a PD (Proportional–Derivative) control for the probe landing on comets. Moreover, an impulsive maneuver control method was designed in Ref. [12] to deal with asteroid's gravitational uncertainties. Lyzhoft et al. conceptually presented a terminal-guidance sensor system for asteroid rendezvous missions [13]. A robust sliding mode predictive control was proposed by Carson et al. [14]. In addition, Zexu et al. [15] investigated an autonomous guidance and control scheme using sliding mode control for probe soft landing on asteroids. A fuzzy sliding mode control scheme was employed for landing phase by Yang et al. [16] then a finite time high-order sliding mode control theory was investigated in Ref. [17] to introduce a nonlinear landing guidance scheme. Lan et al. [18] and Liu et al. [19] used nonsingular terminal sliding mode control approach for finite-time probe soft landing on asteroids. Similarly, terminal sliding mode control was employed for asteroid both hovering and landing by Ynag et al. [20]. In the following, Li et al. investigated trajectory control of a probe for the asteroid landing mission using adaptive fuzzy sliding mode control algorithm [21]. Finally, to improve the safety and reliability of the asteroid landing mission, an active trajectory control-based landing strategy using a convex optimization-based control algorithm was proposed in Ref. [22].

Obviously, reducing the fuel consumption is a priority in space missions. Thus, the employed control framework should minimize the required control effort. Furthermore, the control method should be robust enough to deal with the effects of model uncertainties and disturbances. Model Predictive Control (MPC) is a well-developed and advanced control method that has been attracting the attention of many researchers. The unique feature of MPC is its prediction-based decision making process. Since this method predicts the future over a finite time horizon using a dynamic model and calculates the current system' input by minimizing a cost function, MPC can be categorized as an optimal control method, which might be useful in the space missions.

In recent years, many researchers have tried to take the advantage of using MPC to find new solutions for space missions. For example, the attitude control of an under-actuated spacecraft using MPC is investigated by Mirshams and Khosrojerdi in similar works [23] and [24]. Mirko et al. employed MPC to control the attitude of an all-electric satellite [25]. Myung and Bang used predictive nutation and spin inversion control for a spin-stabilized spacecraft in Ref. [26], and employed Nonlinear Model Predictive Control (N-MPC) to control the attitude of a spacecraft in Ref. [27]. Chen and Wu studied the attitude control of a Cubesat using MPC [28]. Similarly, an automatic differentiation-based N-MPC is developed by Cao et al. for satellite attitude control using magneto-torquers [29]. The adaptive predictive controller with adaptive notch filter for the tip position control of a deployable space structure is addressed in Ref. [30] and Wang at al. studied the advantage of using MPC to control space robot arms [31]. In addition, Soltani et al. used an N-MPC approach to control the libration of the Tethered Space Robot [32]. The model predictive orbit control of a satellite considering different kinds of orbit disturbances is investigated in Ref. [33] and Bai et al. introduced a One-Bit Processing Based Model Predictive Control (OBMPC) algorithm for a fractionated satellite mission to reduce online calculations by removing multiply operations in Ref. [34]. Starek and Kolmanovsky studied the interplanetary mission control using MPC [35]. The spacecraft relative motion guidance and control based on a MPC approach with dynamically reconfigurable constraints is presented in Ref. [36] and Least Absolute Shrinkage and Selection Operator (LASSO) model predictive control is applied to the terminal phase of a spacecraft rendezvous and capture mission in Ref. [37]. Esafahani and Khorasani proposed a distributed MPC as a fault-recovery control scheme for satellite formation flying [38] and Sauter and Palmer developed an MPC-based analytical algorithm for collision-free satellite formation flight maneuvering in Ref. [39].

This study focuses on the asteroid-landing problem using a predictive framework to achieve a safe and accurate landing. Specially, an innovative approach to MPC problem is introduced to deal with the high computational burden. The rest of paper is organized as follows. In Section 2, the general dynamical model of the spacecraft's motion around an asteroid is described. Section 3 illustrates the guidance and control framework for landing on an asteroid in details, and the Predictive Path Planning guidance approach and Multiple-Horizon Multiple-Model Predictive Control are introduced. Then, the performance of the proposed framework is evaluated through numerical simulations in Section 4. Finally, concluding remarks are presented in Section 5.

2. Dynamical model

The gravitational potential field of an asteroid is a function of position in the asteroid-fixed coordinate system. Thus, the equations of motion of a spacecraft about an asteroid are defined in the rotating body-fixed frame.

Fig. 1 shows the model configuration and the coordinate systems. As can be seen, the $O_I x_I y_I z_I$ represents the inertial reference frame and asteroid-fixed coordinate system is denoted by $O_b x_b y_b z_b$ whose origin is located at the asteroid's center of mass and unit axes are aligned along the asteroid's principal axes. $\boldsymbol{R} = [x, y, z]^{\mathrm{T}}$ is the position vector of the spacecraft from the target asteroid's center of mass defined in the asteroid-fixed coordinate system. $\boldsymbol{r_s}$ and $\boldsymbol{r_a}$ are the position vectors of the spacecraft and the asteroid with respect to the inertial reference frame, respectively.

According to the Coriolis principle, the asteroid-fixed equations of motion of the spacecraft about a rotating asteroid are given by

$$\ddot{\boldsymbol{R}} + 2\boldsymbol{\Omega} \times \dot{\boldsymbol{\Omega}} + \boldsymbol{\Omega} \times (\boldsymbol{\Omega} \times \boldsymbol{R}) + \dot{\boldsymbol{\Omega}} \times \boldsymbol{R} = \nabla \boldsymbol{U} + \boldsymbol{F} + \delta \boldsymbol{u} \tag{1}$$

in which $\boldsymbol{\Omega}$ represents the angular velocity vector of the asteroid, $\nabla \boldsymbol{U}$ denotes the gradient vector of the asteroid's gravitational potential field, $\boldsymbol{F}$ is the control acceleration vector and $\delta \boldsymbol{u}$ represents the perturbing acceleration vector which might be caused by the solar radiation pressure, model inaccuracy or other planets gravitational effects.

There are different approach to represent and calculate the gravitational potential of celestial bodies, which can be employed for irregular body shapes. Classically, the gravitational potential of major celestial bodies such as planets and moons are modeled using spherical harmonies series expansion. This method represents the gravitational potential function using a finite series of the associated Legendre functions as follows [40]:

$$U(\boldsymbol{R}) = \frac{GM_B}{R} \sum_{l=0}^{\infty} \sum_{m=0}^{l} \left(\frac{R_B}{R}\right)^l \overline{P}_{l,m}[\sin(\varphi)]\left(\overline{C}_{l,m} \cos(m\lambda) + \overline{S}_{l,m} \sin(m\lambda)\right) \tag{2}$$

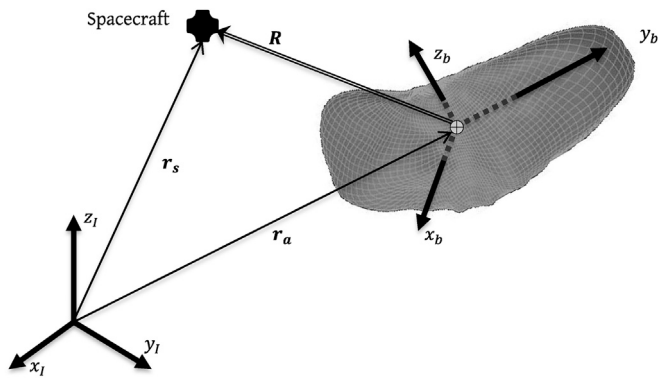

Fig. 1. The model configuration and the coordinate systems.

where G is the Gravitational constant, M_B is the mass of the target body and R_B is the reference radius which is generally the largest equatorial radius. R represents the distance of the spacecraft from the asteroid's center of mass and φ and λ denote the latitude and longitude of the spacecraft in the coordinate system fixed to the asteroid, respectively. $\overline{P}_{l,m}$ is the normalized associated Legendre polynomial of degree l and order m and $\overline{C}_{l,m}$ and $\overline{S}_{l,m}$ are the normalized Stokes' coefficients.

It should be noted that the accuracy of the gravitational model depends on the degree and the order of the spherical harmonics model. Although increasing the degree and the order increases the model's accuracy, it causes high computational burden.

Polyhedron model is an alternative approach to calculate the gravitational potential of irregular body shapes and is computationally expensive. In this method, the target body is considered as a series of polyhedrons that are solid three-dimensional figures and contain vertices, edges and triangular planar surfaces called faces. With the assumption that the polyhedron's density is constant, the gravitational potential is derived as [41].

$$U(\boldsymbol{R}) = \frac{1}{2}G\rho\left(\sum_{e\in\ edge}\boldsymbol{r}_e^T\mathbf{E}_e\boldsymbol{r}_e\cdot\boldsymbol{L}_e - \sum_{f\in\ face}\boldsymbol{r}_f^T\mathbf{F}_f\boldsymbol{r}_f\cdot\boldsymbol{\omega}_f\right) \tag{3}$$

in which ρ is the density of the primary body. $\boldsymbol{r}_f$ and $\boldsymbol{r}_e$ are the position vectors from the spacecraft to any points on surface f and edge e, respectively. $\mathbf{E}_e$ and $\mathbf{F}_f$ are 3×3 dyad matrixes which are defined as

$$\mathbf{F}_f = \widehat{\boldsymbol{n}}_f\widehat{\boldsymbol{n}}_f\mathbf{E}_e = \widehat{\boldsymbol{n}}_{f_i}\widehat{\boldsymbol{n}}^i_{f_{j,i}} + \widehat{\boldsymbol{n}}_{f_j}\widehat{\boldsymbol{n}}^j_{f_{i,j}} \tag{4}$$

where $\widehat{\boldsymbol{n}}_f$ is the normal vector to face f and $\widehat{\boldsymbol{n}}^j_{f_{i,j}}$ is the outward facing normal vector to edge connecting vertices i and j. Furthermore, $\boldsymbol{\omega}_f$ denotes the solid angle for each face defined by the vectors from the spacecraft to its vertexes and is given as

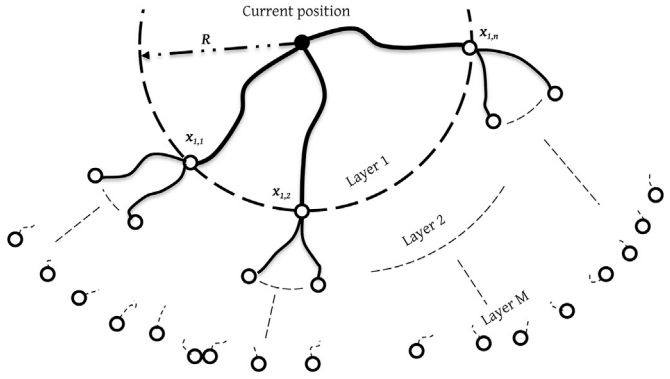

Fig. 2. The outline of the PPP's structure.

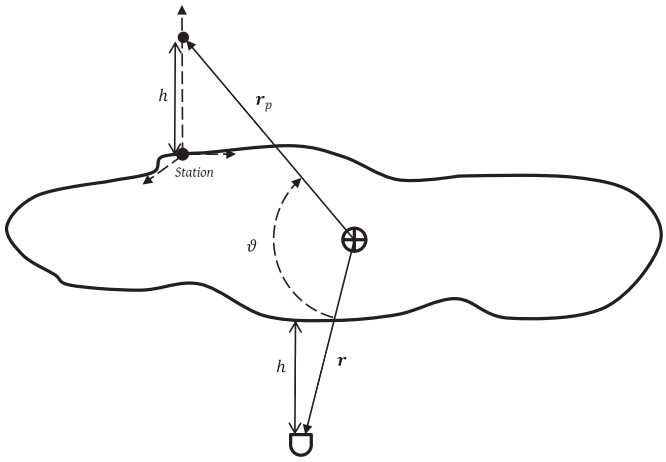

Fig. 3. The landing configuration and predictive guidance parameters.

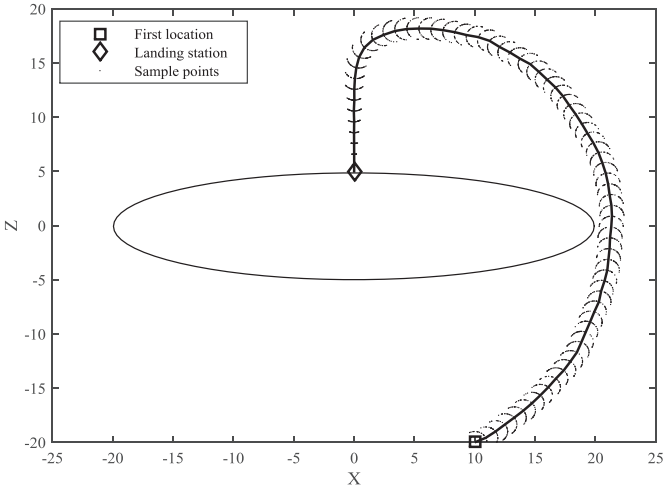

Fig. 4. Typical 2D path planning problem using 40 sample points.

$$\omega_f = 2\tan^{-1}\left(\frac{\boldsymbol{r}_i\cdot(\boldsymbol{r}_j\times\boldsymbol{r}_k)}{r_ir_jr_k + r_i(\boldsymbol{r}_j\cdot\boldsymbol{r}_k) + r_j(\boldsymbol{r}_k\cdot\boldsymbol{r}_i) + r_k(\boldsymbol{r}_i\cdot\boldsymbol{r}_j)}\right) \quad i,j,k = 1,2,3;\ i\neq j\neq k \tag{5}$$

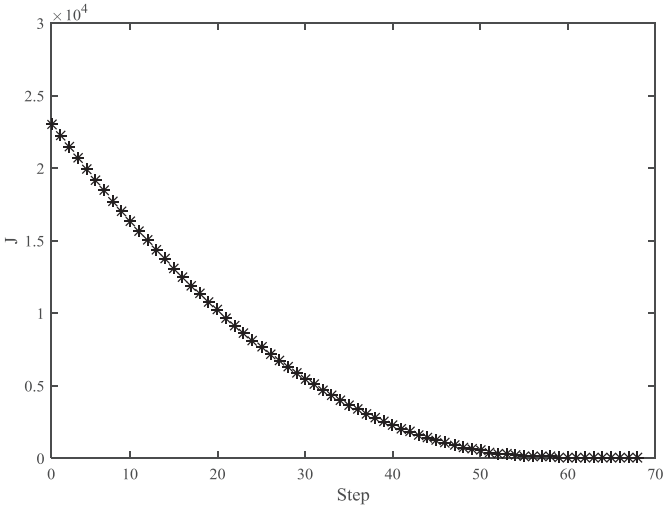

Fig. 5. The cost of the designed path as a function of step.

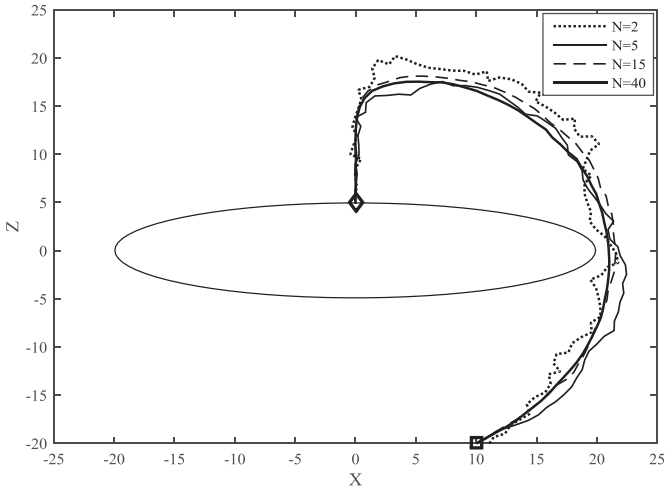

Fig. 6. Comparison of the generated path using different number of sample points.

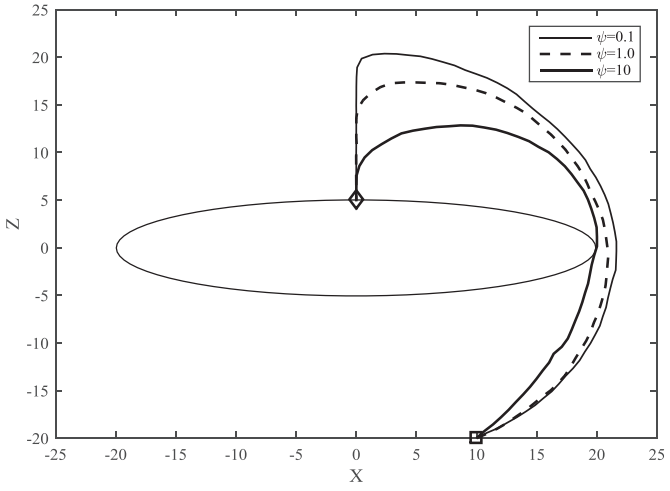

Fig. 7. The effect of ψ on the generated path.

Table 1
433 Eros spherical harmonic coefficients [44].

i	j	$\bar{C}_{i,j}$	$\bar{S}_{i,j}$
0	0	+7.324533540690e+00	+0.000000000000e+00
1	0	−1.202642483560e−01	+0.000000000000e+00
1	1	+1.361912835560e−01	+6.020579170230e−01
2	0	−1.086728029650e+00	+0.000000000000e+00
2	1	−3.339748836320e−02	+2.118272136830e+00
2	2	+6.867572347840e−02	−8.982333315420e−01
3	0	−2.224113245000e−02	+0.000000000000e+00
3	1	+6.007305178040e−02	−2.153846932180e−02
3	2	+1.102471301070e−01	+2.461804673070e−02
3	3	+1.459820815640e−01	−2.901819674960e−01
4	0	+3.660264743290e−01	+0.000000000000e+00
4	1	−5.694634236560e−02	+3.938373154580e−02
4	2	+5.664768324830e−03	+6.690655503620e−02
4	3	−4.355504560990e−01	+4.177942728870e−01
4	4	+2.471335328690e−01	−1.981165431920e−01

and $\boldsymbol{L}_e$ is a function of distances between the spacecraft and each edge with length of e_{ij} defined by $\boldsymbol{r}_i$ and $\boldsymbol{r}_j$ as follows

$$\boldsymbol{L}_e = \ln\left(\frac{r_i + r_j + e_{ij}}{r_i + r_j - e_{ij}}\right) \tag{6}$$

Table 2
The initial and the desired final states of the landing problem.

	Initial Condition	Landing Condition
Position (km)	$[-5 \quad 0 \quad -15]^T$	$[-5 \quad 0.44 \quad 5.43]^T$
Velocity (m/s)	$[0 \quad 40 \quad 0]^T$	$[0 \quad 0 \quad 0]^T$

Table 3
The numerical simulation parameters and algorithm setting.

parameter	N	M	σ^2_{min} (Deg.)	σ^2_{max} (Deg.)	D (km)	**R**
value	20	2	20	50	1	diag($\mathbf{10}_{3\times1}$)
parameter	ψ	dt (s)	v_{max} (m/s)	τ_{max} (s)	ϑ_L (Deg.)	**Q**
value	0.5	0.1	50	400	30	diag($[\mathbf{1}_{3\times1} \quad \mathbf{100}_{3\times1}]$)

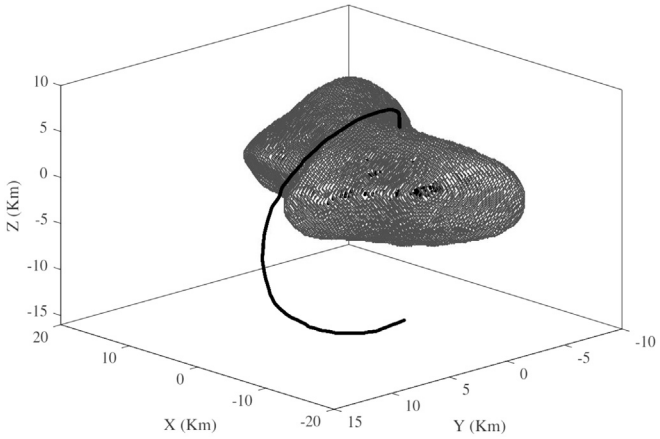

Fig. 8. The planned path in the asteroid-fixed coordinate system.

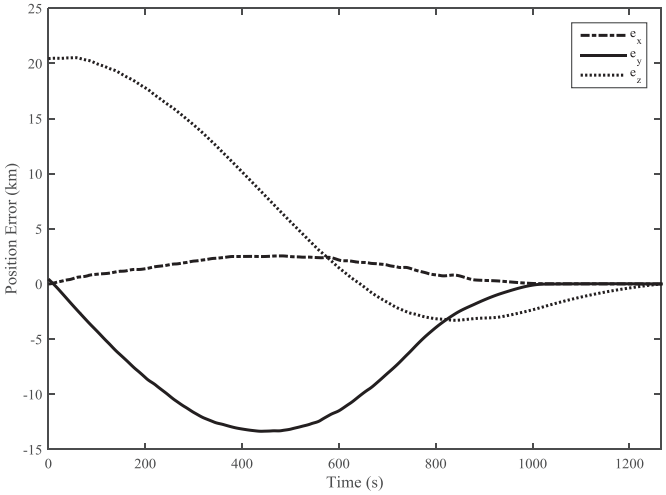

Fig. 9. The planned relative spacecraft's position with respect to the landing site.

3. Guidance and control framework

In this section, a theoretical framework for the asteroid-landing problem in asteroid-fixed coordinate system is introduced. The framework includes two parts; (1) Path planning, and (2) Control law to track the planned path. In this way, Predictive Path Planning method as a randomized-based

heuristic approach is introduced to generate the reference trajectory. Then, the Multiple-Horizon Multiple-Model Predictive Control (MHMM-PC) is introduced and employed to track the reference trajectory. The important advantage of the MHMM-PC approach is reducing the required computational burden. Throughout this section, $\boldsymbol{x}$ represents the Euclidian norm of vector $\boldsymbol{x}$ and $\boldsymbol{x}_{\mathbf{Q}}^2$ is defining the weighted norm of $\boldsymbol{x}$ defined by $\boldsymbol{x}^{\mathrm{T}}\mathbf{Q}\boldsymbol{x}$ where $\mathbf{Q}$ is a positive definite matrix. Moreover, $\mathcal{N}(\mu,\sigma^2)$ denotes the normal distribution with mean μ and variance σ^2.

3.1. Predictive Path Planning

The main goal of this part is to develop a predictive guidance framework, which is applicable to the asteroid-landing problem. The method is developed based on a probabilistic randomized approach. The proposed guidance method, named Predictive Path Planning (PPP), benefits from using the prediction of future states using simple and approximate model. The main objective of this guidance method is to satisfy the constraints and to guarantee a soft vertical landing. Moreover, it is designed to be efficient with low computational burden.

The PPP algorithm with a recurring approach can be summarize as follows:

(1) The current position is selected as the first host point;
(2) Calculate the cost of the host point J_H;
(3) Sample N points $x_i \in \mathbb{R}^3$ from the sample space Σ so that $x_i \in \{\Sigma | J_i < J_H, i = 1,\ldots,N\}$;
(4) Repeat (3) for each new point to generate M layers;
(5) Calculate the decision cost J_{i_D} of each sample point of the first layer $J_D = \sum_{i=1}^{M} w_i \sum_{j=1}^{N^{(i-1)}} J_{i,j}$ where w_i is the weight coefficient of the ith layer;
(6) Select the optimal position as the next host point with minimum J_D;
(7) Generate the approximate trajectory between the current position and the next host point;
(8) Repeat (2) to (7) until the sample space contains the final target point;
(9) Select the target point as the next host point.

Fig. 2 shows the outline of the algorithm. As can be seen, here the sample space Σ is a sphere with radius D. Thus, Σ is defined as:

$$\Sigma \sim D \begin{bmatrix} cos\theta cos\phi \\ sin\theta cos\phi \\ sin\phi \end{bmatrix}, \quad \begin{matrix} 0 \le \theta \le 2\pi \\ -\frac{\pi}{2} \le \phi \le \frac{\pi}{2} \end{matrix} \tag{7}$$

where variables θ and ϕ are the azimuthal coordinate and the polar coordinate, respectively. Generally, the searching process for sample points could be done fully random or based on a probability distribution function (PDF). In other words, the searching process is affected by the distribution functions of sample space's variables.

Let μ_θ be the azimuthal coordinate and μ_ϕ be the polar coordinate of the velocity vector of the host point. To generate a smooth trajectory and consider the spacecraft's inertia, the sample space's variables are considered as $\theta \sim \mathcal{N}(\mu_\theta, \sigma_\theta^2)$ and $\phi \sim \mathcal{N}(\mu_\phi, \sigma_\phi^2)$ which have normal PDFs where σ^2 can be defined as a linear function of velocity v as $\sigma^2 = \sigma_{\max}^2 + \frac{\sigma_{\min}^2 - \sigma_{\max}^2}{v_{max}} v$ in which v_{max} is the maximum allowable velocity and the searching variance is bounded on $\left[\sigma_{\min}^2 \quad \sigma_{\max}^2\right]$. It is noteworthy that the relative position vector of each layer's points with respect to their host point can be taken as their virtual velocity vectors, which are needed to generate the next layer.

The cost function plays the key role in planning a suitable path. As mentioned before, one of the main objectives of the guidance algorithm is to drive the probe so that it lands vertically. Moreover, the landing accuracy and the soft landing approach are indispensable. Thus, the cost of each point that is the decision-making criteria should be defined in such a way to satisfy all remarked demands. In this way, the cost function of each sample point is defined as follows:

$$\begin{matrix} \min\left\{ J = \|\vartheta(\boldsymbol{r})\|^2 + \|h(\boldsymbol{r})\|_{\psi}^2 \right\} \\ \text{subject to}\{g(\boldsymbol{r}) < 0\} \end{matrix} \tag{8}$$

where h is the altitude of the position vector $\boldsymbol{r}$, and ϑ is the angle between the position vector and a virtual point position vector $\boldsymbol{r}_p$ with altitude h above the landing station. In addition, ψ represents the relative scalar positive weighting coefficient. $g(\boldsymbol{r})$ is defining the collision constraint that prevents the probe from hitting the asteroid. The introduced parameters are shown in Fig. 3.

Fig. 4 shows a 2D sample path-planning problem. 40 sample points and one layer are considered to generate the guidance path. Moreover, the admissible sample space is a 1 distance unit radius circle and $\psi = 1$. It is obvious that the resulted smooth path has reached the landing station successfully in the vertical direction and the collision avoidance constraint is effectively satisfied. Furthermore, the monotonic decreasing trend of the cost function is demonstrated in Fig. 5, where it can be seen that the cost function converges to zero in 68 steps.

It should be noted that the quality of the generated path is related to the value of the relative weight ψ as well as the number of the sample points (N) and layers (M). N and M adjust the smoothness of the path and ψ controls the vertical landing condition. Fig. 6 compares the generated paths using different number of sample points. Obviously, more smoothness could be obtained by increasing the number of sample points. Although, it causes high computational burden.

The difference between planed paths with different ψ is demonstrated in Fig. 7. As shown in this figure, the vertical landing part of the trajectory lengthens with decrease in the relative weight ψ. Furthermore, the probability of hitting asteroid decreases by choosing a small enough value of ψ.

The last step to generate a smooth planned trajectory is connecting calculate terminal points by a polynomial as a function of time. This way, the following cubic polynomial trajectory is employed between each two consecutive points:

$$\begin{aligned} \boldsymbol{r}(t) &= \boldsymbol{r}_0 + \dot{\boldsymbol{r}}_0 t - \left(3\boldsymbol{r}_0 - 3\boldsymbol{r}_f + 2\dot{\boldsymbol{r}}_0\tau + \dot{\boldsymbol{r}}_f\tau\right)\frac{t^2}{\tau^2} + \left(2\boldsymbol{r}_0 - 2\boldsymbol{r}_f + \dot{\boldsymbol{r}}_0\tau + \dot{\boldsymbol{r}}_f\tau\right)\frac{t^3}{\tau^3} \\ \dot{\boldsymbol{r}}(t) &= \dot{\boldsymbol{r}}_0 - \left(6\boldsymbol{r}_0 - 6\boldsymbol{r}_f + 4\dot{\boldsymbol{r}}_0\tau + 2\dot{\boldsymbol{r}}_f\tau\right)\frac{t}{\tau^2} + \left(6\boldsymbol{r}_0 - 6\boldsymbol{r}_f + 3\dot{\boldsymbol{r}}_0\tau + 3\dot{\boldsymbol{r}}_f\tau\right)\frac{t^2}{\tau^3} \end{aligned} \tag{9}$$

where $\tau = \frac{2D}{|\dot{\boldsymbol{r}}_f| + |\dot{\boldsymbol{r}}_0|} < \tau_{max}$ is the specified time interval of each polynomial patch. $\boldsymbol{r}_0$ and $\dot{\boldsymbol{r}}_0$ denote the initial position (host point) and velocity

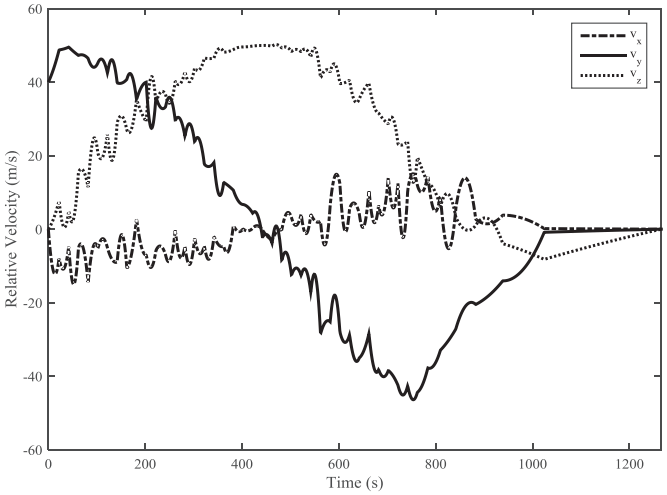

Fig. 10. The planned relative spacecraft's velocity with respect to the landing site.

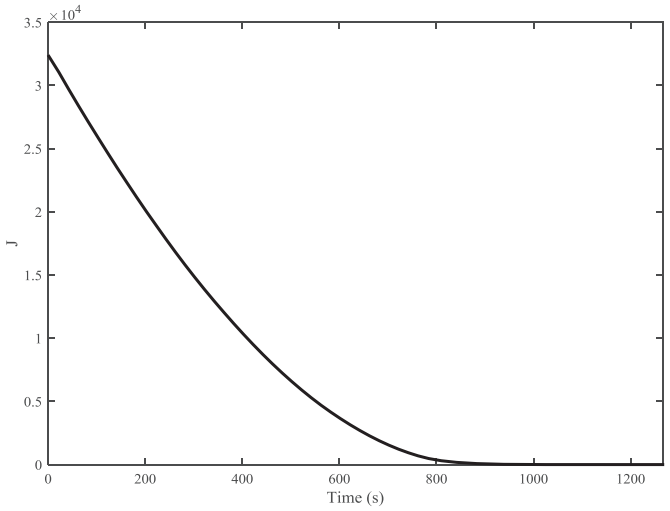

Fig. 11. The cost of the planned landing path as a function of time.

vectors, respectively. $\boldsymbol{r}_f$ and $\dot{\boldsymbol{r}}_f$ represent the planned position (next host point) and its desired velocity vector.

A switch function is employed to determine $\dot{\boldsymbol{r}}_f$. The relative position vector of the best point of the second layer to the next host point ($\boldsymbol{r}_f$) is taken as the direction of $\dot{\boldsymbol{r}}_f$. The probe's trajectory can be separated into two different parts; the transition part to the top of the landing site, and the soft vertical landing part. Whereas the major specification of the first part is that, the probe has to move fast, the soft landing should be guaranteed during the second part. Thus, the magnitude of $\dot{\boldsymbol{r}}_f$ can be designed as follows:

$$\left|\dot{\boldsymbol{r}}_f\right| = \begin{cases} v_{\max} & \vartheta > \vartheta_L \\ v(h) & \vartheta \leq \vartheta_L \end{cases} \tag{10}$$

where $v_{\max}$ is the maximum admissible velocity of the probe, ϑ_L is the half-angle of the landing zone cone, and $v(h)$ is the spacecraft's velocity in the second part as a linear function of altitude $v(h) = v_{\max} h/h_L$, in which h_L is the spacecraft's altitude at the moment of arrival to the landing zone cone.

3.2. Multiple-Horizon Multiple-Model Predictive Control

MPC has an attractive and flexible structure to deal with control uncertain problems that are needed to be optimum in terms of a predefined performance index. The basic idea of MPC is employing a model to predict the system's outputs over a finite time horizon as well as an online performance index optimization to calculate the control sequence so that certain constraints are also satisfied. The prediction and optimization processes are performed at each time instant and the first element of the calculated control input sequence is applied to the system and the whole procedure should be repeated at the next time step.

N-MPC refers to each MPC approach, which uses nonlinear dynamical model to predict the future output. Although, the fundamental structure of the MPC remains the same, an N-MPC causes several difficulties such as turning the optimization problem into a non-convex problem and the stability of the closed-loop system. However, making the prediction and optimization processes time consuming is the major difficulty of the N-MPC, which makes it hard to implement for online applications.

As it is mentioned in the Section 2, although polyhedron method is the most accurate mathematical model to calculate the gravitational field of an irregular shape celestial body, it is a nonlinear computationally expensive method. Thus, the N-MPC in conjunction with the polyhedron formulation as the prediction model has high computational complexity. Therefore, a different approach is needed to handle computationally expensive MPC problems. MHMM-PC is a method with the capability of reducing the computational burden, while the performance of the controlled system remains satisfactory.

The general objective of MPC problems is optimizing a cost function including the control effort cost and the reference trajectory tracking cost which is generally given as follows [42]:

$$J = \sum_{i=N_1}^{N_2} \|\widehat{\boldsymbol{y}}_{t+i} - \boldsymbol{w}_{t+i}\|_{\mathbf{Q}}^2 + \sum_{i=1}^{N_u} \|\boldsymbol{u}_{t+i-1}\|_{\mathbf{R}}^2 \tag{11}$$

in which $\widehat{\boldsymbol{y}}$ and $\boldsymbol{w}$ are the predicted output and the reference trajectory

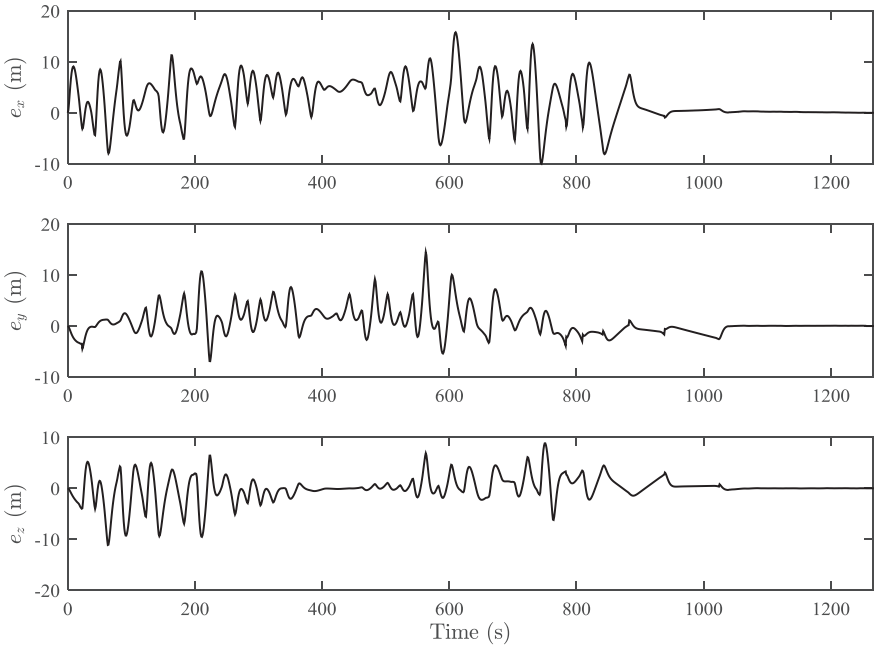

Fig. 12. The controlled position error with respect to the reference trajectory using MHMM-PC.

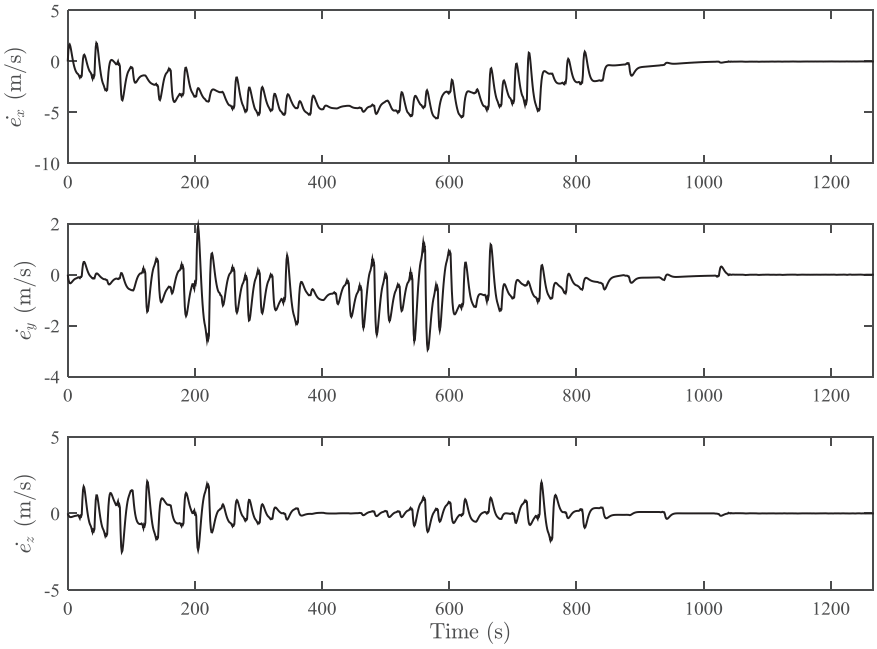

Fig. 13. The controlled velocity error with respect to the reference trajectory using MHMM-PC.

vectors, respectively, and $\boldsymbol{u}$ is the control effort sequence vector. Moreover, N_1 and N_2 denote the lower and upper limits of the prediction horizon, respectively, and N_u represents the length of the control sequence.

Although the most available accurate dynamics model is usually employed to predict the system's future output in MPC problem, studies show that detailed information of the distant future affect the calculated control effort negligibly. In other words, the applied control effort at each time instant is less influenced by the detailed information of the far future than close future. However, some uncertain but significant parts of data in the far future might have considerable effects on the calculated control sequence. Since the importance of accuracy decreases as the length of time horizon increase, inexact but valuable prediction model can be employed as the prediction model for far future. This way, the computational complexity might decrease, while the performance remains acceptable. This is the main idea of the Multiple-Horizon Multiple-Model Predictive Control (MHMM-PC).

MHMM-PC approach uses $\mathscr{M}$ consecutive time horizons instead of one time horizon and implements the most accurate prediction model in the close future and approximate prediction models in the far future. Consequently, the cost function of MHMM-PC approach can be defined as:

$$J = \sum_{i=1}^{\mathscr{M}} \left(\sum_{j=N_{1|i}}^{N_{2|i}} \left\| \boldsymbol{e}_{t+j|t} \right\|_{\mathbf{Q}}^2 + \sum_{j=1}^{N_{u|i}} \left\| \boldsymbol{u}_{t+j-1|t} \right\|_{\mathbf{R}}^2 \right) \tag{12}$$

where $\mathscr{M}$ is the number of horizons and it means that $\mathscr{M}$ different

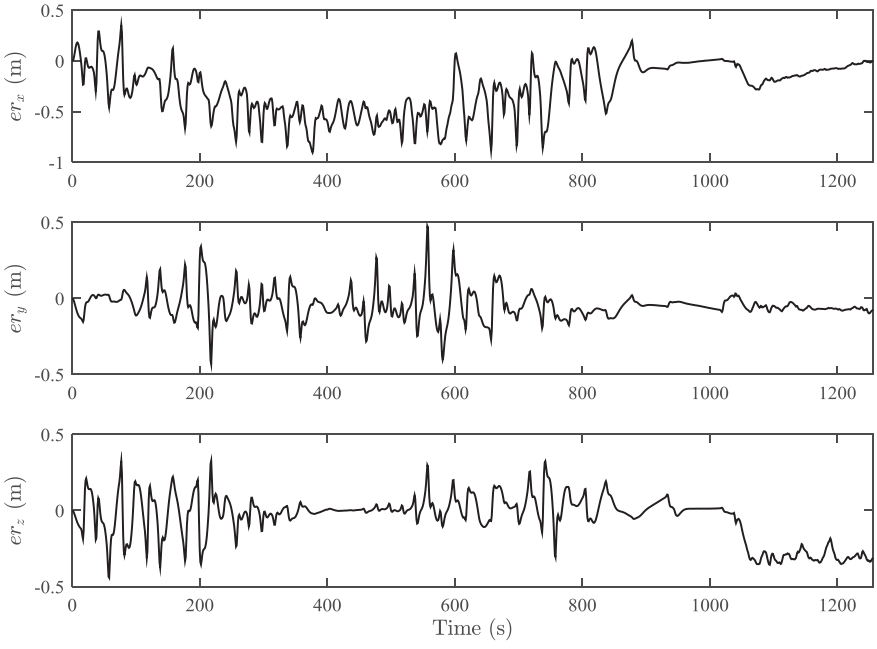

Fig. 14. The difference of controlled position using MHMM-PC and MPC approaches.

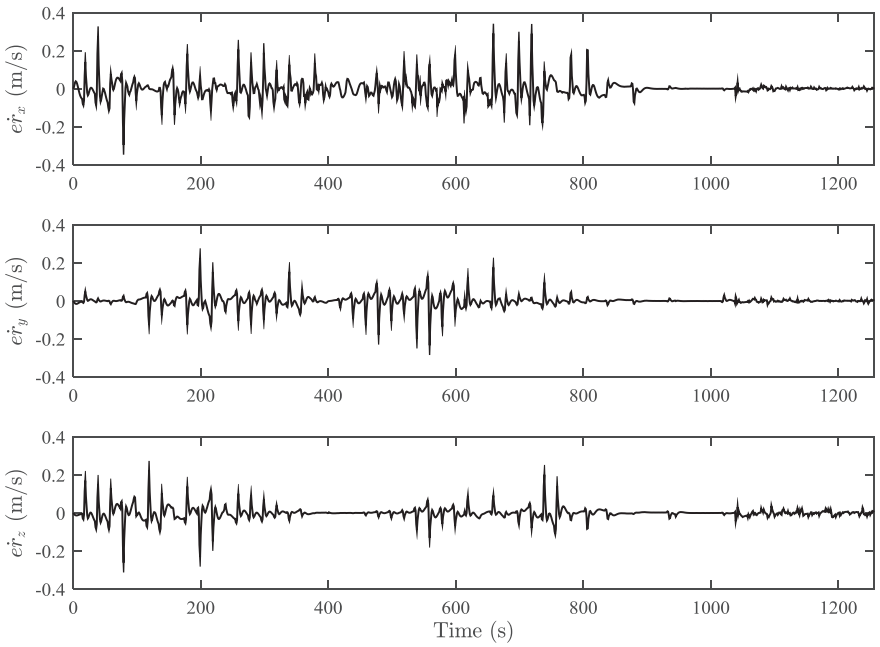

Fig. 15. The difference of controlled velocity using MHMM-PC and MPC approaches.

prediction models are employed, $\boldsymbol{e}_i$ and $\boldsymbol{u}_i$ denote the output error vector with respect to the reference trajectory and the control input vector of the i th prediction model, respectively. The length of each horizon is specified by $N_{1|i}$ and $N_{2|i}$. Also, $N_{u|i}$ represents the length of each control sequence. Since the sum of the length of time horizons in MHMM-PC is equal to the length of one time-horizon in MPC, MHMM-PC turns to MPC when $\mathscr{M} = 1$.

4. Numerical simulation

In this section, the performance of the introduced approach is investigated using numerical simulations. Rotational Asteroid 433 Eros is considered as the target body that is the second-largest near-Earth asteroid, 34.4 × 11.2 × 11.2 km in size, its mean density is 2.67 g/cm^3, and the spin rate is equal to 3.312e-4 rad/s [43]. The employed models are from Planetary Data System of NASA [44]. The polyhedron model is formed of 49152 faces and the spherical harmonic coefficients of the asteroid are listed in Table 1. It is assumed that the asteroid's spin vector axis is directed along its third body-fixed axis. The initial state of the spacecraft and landing station position described in the asteroid-fixed coordinate system are presented in Table 2. To investigate the disturbance rejection ability of the proposed method, the solar radiation pressure perturbation is modeled as well as a disturbance acceleration vector $\delta\boldsymbol{u} = 1.5 \times 10^{-3}\,\sin(t)\mathrm{m/s}^2$ [19] is applied to the system. It should be noted that these two disturbance accelerations are not considered in the prediction models. Furthermore, it is assumed that the polyhedrons' actual density has a normal distribution as $\rho_i \sim \mathscr{N}(\rho, 0.05)$ and there is 10% error in mass of the prediction model with respect to the real model.

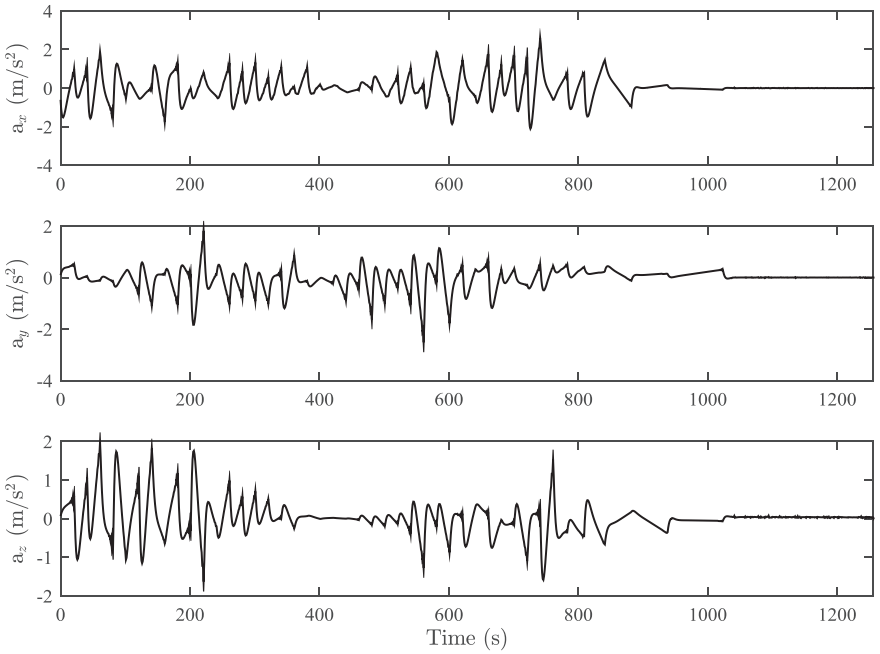

Fig. 16. The calculated required control acceleration using MHMM-PC.

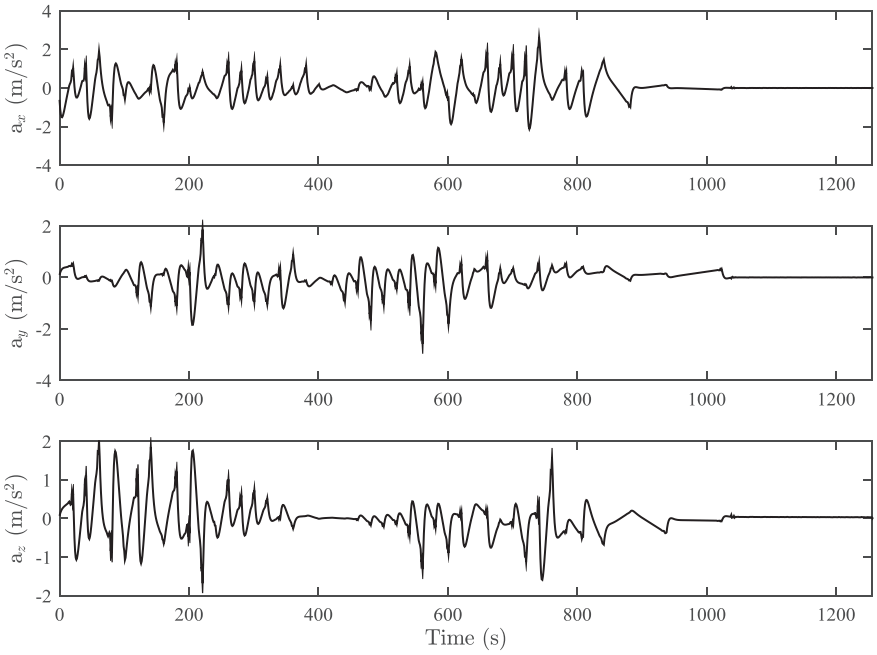

Fig. 17. The calculated required control acceleration using MPC.

To solve the landing problem, MPC and MHMM-PC approaches with the total prediction horizon of 10 s are employed. The MPC approach uses polyhedron gravitational model for prediction and the horizon's time step is 1 s. The MHMM-PC approach employs two different horizons. In the first 4-s horizon, the polyhedron gravitational model is utilized for prediction with 1-s time steps. The spherical harmonics model is used as the prediction model over the remaining 6-s horizon with 3-s time step. The simulation parameters and the setting of guidance and control framework are listed in Table 3. It is noteworthy that the fourth-order Runge-Kuta algorithm is employed for the numerical integrations and the Sequential Quadratic Programming (SQP) algorithm is employed to solve the optimization problems. Furthermore, the computation time is measured on a CORE i7 4.00 GHz CPU computer with 32 GB RAM.

Fig. 8 shows the planned path in the asteroid-fixed coordinate system where the vertical landing part is evident. The spacecraft's position error with respect to the landing site and its relative velocity as functions of time are shown in Figs. 9 and 10, respectively. As it can be seen in these figures, the spacecraft reaches the landing site at zero velocity. In addition, it is clear that during the final landing part, the spacecraft moves vertically and the relative velocity decreases smoothly. Fig. 11 demonstrates the monotonic decreasing trend of the PPP cost function and its convergence to zero in a finite time. The controlled position and velocity error with respect to the reference-planned trajectory using MHMM-PC are illustrated in Figs. 12 and 13, respectively. It is obvious that the proposed controller is able to drive the spacecraft to track the reference trajectory successfully so that the position error is less that 20 m and the maximum velocity error is about 5 m/s. While during the final landing part, the control approach is able to stabilize the tracking error so that the position and the velocity error of the landing phase are less than 0.1 m and 0.01 m/s, respectively.

It is noteworthy that the system's outputs using MPC and MHMM-PC are very similar. Figs. 14 and 15 show the difference of system's outputs using two approaches ($\boldsymbol{er} \triangleq \boldsymbol{y}_{\mathrm{MHMM-PC}} - \boldsymbol{y}_{\mathrm{MPC}}$). As it can be seen, the position difference is less that 1 m and the velocity difference is less than 0.5 m/s. Similarly, the fact is verified by Figs. 16 and 17 that reducing the model accuracy in the far future does not make an effective change in the system's performance including output and calculated input command at each time instant.

Finally, the performances of the approaches are compared in Table 4. Clearly, two approaches have similar total performance index including integral of control effort and the position error with respect to the reference trajectory. Although, the MPC approach consumes slightly less energy (about 0.3%) and the integral of position error of MHMM-PC approach is 1.4% more than MPC. However, the main advantage of using the MHMM-PC over the MPC is apparently reduction in the computational time. Using the conventional MPC approach needs almost 4 times more computational time than proposed MHMM-PC method.

Table 4
Comparison of system's performance using MPC and MHMM-PC.

Method	MPC	MHMM-PC
$\int \lvert \boldsymbol{e} \rvert \, dt(m)$	8345.8	8463.3
$\int \boldsymbol{F}^T \boldsymbol{F} dt(m/s^2)^2$	838.59	841.53
Computational time (Hr.)	28.98	7.46

5. Conclusion

A predictive framework including guidance and control law for soft landing on an asteroid is presented. Presented recursive Predictive Path Planning algorithm guarantees an accurate vertical landing in a finite time and prevents the spacecraft from hitting the asteroid. The Multiple-Horizon Multiple-Model Predictive Control approach as a different variation of Model Predictive Control is employed to deal with landing problem's high computational burden. This way, it is proven that not all information is needed to make the right decision and it could be possible to reduce the computational complexity without lack of performance. The results of a numerical scenario regarding landing on Asteroid 433 Eros are presented which demonstrate the effectiveness of the proposed framework in keeping the optimality, decreasing the computational burden and rejecting the disturbances and unmolded dynamics influences.

References

[1] J. Bellerose, A. Girard, D.J. Scheeres, Dynamics and control of surface exploration robots on asteroids, in: Optimization and Cooperative Control Strategies, vol. 381, Springer Berlin Heidelberg, Berlin, 2009, pp. 135–150.
[2] C. Lewicki, P. Diamandis, E. Anderson, C. Voorhees, F. Mycroft, Planetary resources—The asteroid mining company, New Space 1 (2) (2013) 105–108.

[3] J. Bell, J. Mitton, Asteroid Rendezvous: NEAR Shoemaker's Adventures at Eros, Cambridge University Press, 2002.
[4] O. Norton, L. Chitwood, Field Guide to Meteors and Meteorites, Springer Science & Business Media, 2008.
[5] E. Hand, Philae probe makes bumpy touchdown on a comet, Science 346 (6212) (2014) 900–901.
[6] J.D. Lafontaine, Autonomous spacecraft navigation and control for comet landing, J. Guid. Control Dyn. 15 (3) (1992).
[7] C. Kluever, Comet rendezvous mission design using solar electric propulsion spacecraft, J. Spacecr. Rockets 37 (5) (2000) 698–700.
[8] D.-C. Liaw, C.-C. Cheng, Variable structure control scheme for landing on a celestial object, Int. J. Syst. Sci. 32 (3) (2001) 295–301.
[9] D. Liaw, C. Cheng, Y. Liang, Three-dimensional guidance law for landing on a celestial object, J. Guid. Control Dyn. 25 (3) (2000) 890–892.
[10] H.-T. Cui, X.-Y. Shi, P.-Y. Cui, Guidance and control law for soft landing asteroid, J. Flight Dyn. 20 (2002) 35–38.
[11] L. Shuang, C. Pingyuan, Landmark tracking based autonomous navigation schemes for landing spacecraft on asteroids, Acta Astronaut. 62 (6–7) (2008) 391–403.
[12] P.-Y. Cui, S.-Y. Zhu, H.-T. Cui, Autonomous impulse maneuver control method for soft landing, J. Astronaut. 29 (2008) 121–126.
[13] J. Lyzhoft, J. Basar, B. Wie, A new terminal guidance sensor system for asteroid intercept or rendezvous missions, Acta Astronaut. 119 (2016) 147–159.
[14] J. Carson, B. Acikmese, R. Murray, D. MacMynowski, Robust model predictive control with a safety mode: applied to small-body proximity operations, in: Proceedings of the AIAA Guidance, Navigation and Control Conference and Exhibit, Honolulu, Hawaii, USA, 2008.
[15] Z. Zexu, W. Weidong, L. Litao, H. Xiangyu, C. Hutao, L. Shuang, C. Pingyuan, Robust sliding mode guidance and control for soft landing on small bodies, J. Frankl. Inst. 349 (2) (2012) 493–509.
[16] Y.-N. Yang, J. Wu, W. Zheng, Trajectory tracking for an autonomous airship using fuzzy adaptive sliding mode control, J. Zhejiang Univ. Sci. 13 (7) (2012) 534–543.
[17] R. Furfaro, D. Cersosimo, D.R. Wibben, Asteroid precision landing via multiple sliding surfaces guidance techniques, J. Guid. Control Dyn. 36 (4) (2013) 1075–1092.
[18] Q. Lan, S. Li, J. Yang, L. Guo, Finite-time soft landing on asteroids using nonsingular terminal sliding mode control, Trans. Inst. Meas. Control 36 (2) (2014) 216–223.
[19] K. Liu, F. Liu, S. Wang, Y. Li, Finite-time Spacecraft's soft landing on asteroids using PD and nonsingular terminal sliding mode control, Math. Probl. Eng. (2015) 1–10.
[20] H. Yang, X. Bai, H. Baoyin, Finite-time control for asteroid hovering and landing via terminal sliding-mode guidance, Acta Astronaut. 132 (2017) 78–89.
[21] Y. Li, H. Wang, B. Zhao, K. Liu, Adaptive fuzzy sliding mode control for the probe soft landing on the asteroids with weak gravitational field, Math. Probl. Eng. (2015) 1–8.
[22] P. Cui, Y. Liu, Z. Yu, S. Zhu, W. Shao, Intelligent landing strategy for the small bodies: from passive bounce to active trajectory control, Acta Astronaut. 137 (2017) 232–242.
[23] M. Mirshams, M. Khosrojerdi, Attitude control of an underactuated spacecraft using tube-based MPC approach, Aerosp. Sci. Technol. 48 (2016) 140–145.
[24] M. Mirshams, M. Khosrojerdi, Attitude control of an underactuated spacecraft using quaternion feedback regulator and tube-based MPC, Acta Astronaut. 132 (2017) 143–149.
[25] M. Leomanni, A. Garulli, A. Giannitrapani, All-electric spacecraft precision pointing using model predictive control, J. Guid. Control Dyn. 38 (1) (2015) 161–168.
[26] H.-S. Myung, H. Bang, Predictive nutation and spin inversion control of spin-stabilized spacecraft, J. Spacecr. Rockets 47 (6) (2010) 1010–1022.
[27] H.-S. Myung, H. Bang, Nonlinear predictive attitude control of spacecraft under external disturbances, J. Spacecr. Rockets 40 (5) (2003) 696–699.
[28] X. Chen, X. Wu, Model predictive control of cube satellite with magnetotorquers, in: Proceedings of the 2010 IEEE International Conference on Information and Automation, Harbin, China, 2010.
[29] Y. Cao, W.-H. Chen, Variable sampling-time nonlinear model predictive control of satellites using magneto-torquers, Syst. Sci. Control Eng. 2 (1) (2014) 593–601.
[30] C.-S. Oh, H. Bang, Deployable space structure control using adaptive predictive controller with notch filter, Aerosp. Sci. Technol. 13 (8) (2009) 459–465.
[31] M. Wang, J. Luob, U. Walter, A non-linear model predictive controller with obstacle avoidance for a space robot, Adv. Asteroid Space Debris Sci. Technol. Part 2 57 (8) (2016) 1737–1746.
[32] M. Soltani, M. Keshmiri, A.K. Misra, Dynamic analysis and trajectory tracking of a tethered space robot, Acta Astronaut. 128 (2016) 335–342.
[33] M. Tavakoli, N. Assadian, Model predictive orbit control of a Low Earth Orbit satellite using Gauss's variational equations, Proc. Inst. Mech. Eng. Part G J. Aerosp. Eng. 228 (13) (2013) 2385–2398.
[34] X. Bai, X. Wu, 1-Bit processing based model predictive control for fractionated satellite missions, Acta Astronaut. 95 (2014) 37–50.
[35] J.A. Starek, I.V. Kolmanovsky, Nonlinear model predictive control strategy for low thrust spacecraft missions, Optim. Control Appl. Methods 35 (1) (2012) 1–20.
[36] A. Weiss, M. Baldwin, R. Scott Erwin, I. Kolmanovsky, Model predictive control for spacecraft rendezvous and docking: strategies for handling constraints and case studies, IEEE Trans. Control Syst. Technol. 23 (4) (2015) 1638–1647.
[37] E. Hartley, M. Gallieri, J. Maciejowski, Terminal spacecraft rendezvous and capture with LASSO model predictive control, Int. J. Control 86 (11) (2013) 2104–2113.
[38] N.R. Esfahani, K. Khorasani, A distributed model predictive control (MPC) fault reconfiguration strategy for formation flying satellites, Int. J. Control 89 (5) (2016) 960–983.
[39] L. Sauter, P. Palmer, Analytic model predictive controller for collision-free relative motion reconfiguration, J. Guid. Control Dyn. 35 (4) (2012) 1069–1079.
[40] W. Kaula, Theory of Satellite Geodesy: Applications of Satellites to Geodesy, vol. 25, Blaisdell Publishing Company, Waltham, Massachusetts, 1966.
[41] R. Werner, A. Scheeres, Exterior gravitation of a polyhedron drived and compared with harmonic and mascon gravitation representations of Asteroid 4769 Castalia, Celest. Mech. Dyn. Astron. 65 (3) (1997) 313–344.
[42] E. Camacho, C. Bordons, Model Predictive Control, second ed., Springer, 2007.
[43] J. Veverka, M. Robinson, P. Thomas, S. Murchie, J. Bell III, N. Izenberg, C. Chapman, A. Harch, M. Bell, B. Carcich, A. Cheng, B. Clark, D. Domingue, D. Dunham, R. Farquhar, M. Gaffey, E. Hawkins, J. Joseph, R. Kirk, H. Li, Lucey, NEAR at Eros: imaging and spectral results, Science 289 (5487) (2000) 2088–2097.
[44] P. Thomas, J. Joseph, B. Carcich, A. Raugh, NEAR MSI Shape Model for 433 EROS V1.0, NEAR-A-MSI-5-EROS-SHAPE-MODELS-V1.0, NASA Planetary Data System, 2001.